



Area and width functions of river networks: New results on multifractal properties

Bruno Lashermes¹ and Efi Foufoula-Georgiou¹

Received 14 July 2006; revised 20 May 2007; accepted 6 June 2007; published 11 September 2007.

[1] This paper investigates the multiscale statistical structure of the area and width functions of simulated and real river networks via state-of-the-art wavelet-based multifractal (MF) formalisms. First, several intricacies in performing MF analysis of these signals are discussed, and a robust framework for accurate estimation of the MF spectrum is presented. Second, it considers the following three questions: (1) Does the topology of river networks leave a unique signature on the MF spectrum of area and width functions? (2) How different are the MF properties of commonly used simulated trees and those of real river networks? and (3) Are there differences between the MF properties of width and area functions, and what can these tell us about the topology of hillslope versus channelized drainage patterns in a river basin? The results indicate discrepancies between the statistical scaling of the area functions of real networks (found to be multifractal with a considerable spread of local singularities and the most prevailing singularity ranging from 0.4 to 0.8) and that of several commonly used stochastic self-similar networks (found to be monofractal with a single singularity exponent H in the range of 0.5–0.65). Moreover, differences are found between the MF properties of width and area functions of the same basin. These differences may be the result of distinctly different branching topologies in the hillslope versus channelized drainage paths and need to be further investigated.

Citation: Lashermes, B., and E. Foufoula-Georgiou (2007), Area and width functions of river networks: New results on multifractal properties, *Water Resour. Res.*, 43, W09405, doi:10.1029/2006WR005329.

1. Introduction

[2] The width function of a river network is a one-dimensional function which summarizes the two-dimensional branching structure of the river network. It represents the distribution of travel distances through the network and, under the assumption of constant flow velocity, the probability distribution of traveltimes. Thus its significance for understanding the hydrologic response of basins and the scaling characteristics of streamflow hydrographs is important. The link of hydrologic response and channel network topology via the width function has been recognized early on. For example, see Kirkby [1976], Troutman and Karlinger [1985], Gupta *et al.* [1986], and Gupta and Mesa [1988], who proposed a width function formulation of the geomorphologic unit hydrograph (GUH). These studies focused on the low-frequency component of the width function which exhibits a similarity to the shape of the instantaneous unit hydrograph. More recently, interest has been expressed in the high-frequency component of the width function and especially its multiscaling properties. This paper is a contribution in this direction.

[3] The width function $W(x)$ is defined as the number of channelized pixels at a flow distance $0 \leq x \leq L$ from the

basin outlet, where L is the length of the longest channelized path in the network, i.e.,

$$W(x) = \#\{\text{channelized } M : x \leq l(M) \leq x + dx\}, \quad (1)$$

where $l(M)$ is the flow distance of pixel M from the outlet and dx is the scale of “coarsening.” Typically the distance x is normalized by L (in which case the support of $W(x)$ is between 0 and 1) and $W(x)$ is normalized by the total number of pixels rendering it a density. For a given network topology, $W(x)$ can be viewed as a stochastic process indexed by the distance x .

[4] Another function of interest is the so-called area function $A(x)$ defined as the number of pixels, not necessarily channelized, at a flow distance x from the basin outlet:

$$A(x) = \#\{\text{all } M : x \leq l(M) \leq x + dx\}. \quad (2)$$

[5] It is noted that $A(x)$ does not require the extraction of the channel network from DEMs, a task that still faces the challenge of specifying the channel initiation processes [e.g., Montgomery and Dietrich, 1988; Montgomery and Foufoula-Georgiou, 1993], and reflects both the channelized and unchannelized (hillslope) parts of the basin.

[6] Several previous works have studied, analytically or via numerical simulation, the statistical scaling properties of $W(x)$ or $A(x)$ for tree topologies such as the Peano basin, Shreve’s random topology model, and self-similar trees (SSTs) as well as real river networks [e.g., Troutman and

¹St. Anthony Falls Laboratory and National Center for Earth-Surface Dynamics, Department of Civil Engineering, University of Minnesota—Twin Cities, Minneapolis, Minnesota, USA.

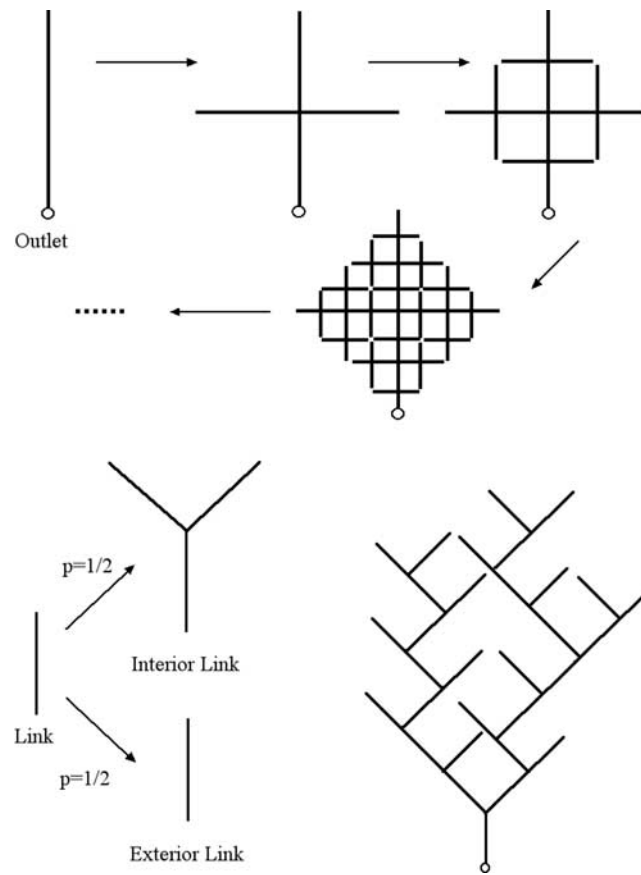


Figure 1. (top) Peano's basin and (bottom) Shreve's random network construction schemes.

Karlinger, 1984, 1985; Marani *et al.*, 1991, 1994; Rinaldo *et al.*, 1993; Veneziano *et al.*, 1995; Gupta and Waymire, 1996; Agnese *et al.*, 1998; Yang *et al.*, 2001; Richards-Pecou, 2002]. Following earlier work of Troutman and Karlinger [1984], Gupta *et al.* [1986], and Gupta and Mesa [1988], recent studies have provided a renewed interest in using simulated river networks and corresponding width functions in efforts to understand, via hydrologic simulation or theoretical derivations, the physical origin of the scaling of floods as arising from the known scaling structure of rainfall and the known fractal properties of river networks [e.g., Menabde *et al.*, 2001; Troutman and Over, 2001].

[7] Given the increasing importance of $W(x)$ and $A(x)$ in hydrogeomorphologic studies, the questions considered in this work are the following: (1) Does the topology of river networks leave a unique signature on the MF properties of the area and width functions? (2) How different are the MF properties of commonly used simulated trees and those of real river networks? and (3) Are there differences between the MF properties of width and area functions and what can these differences tell us about the topology of hillslope versus channelized drainage patterns in a river basin?

[8] The ability to answer the above questions heavily relies on using the correct tools for MF analysis. Veneziano *et al.* [1995] pointed out some deficiencies in using the standard techniques of MF analysis for width functions, mainly addressing the nonstationary nature of these signals. In this paper, we present a robust framework for MF analysis of width and area functions which (1) offers accurate estimates of the MF spectrum without the need

to know a priori the intrinsic nature of the analyzed signal (i.e., measure versus function) and the form of nonstationarity (linear versus higher-order trends) and (2) offers a concise parameterization of multifractality (two parameters only) even for short signals for which high-order moments are unreliable. We use this framework to point out important differences between the MF properties of simulated and real river networks. Specifically, we show that the width function of real networks has a richer MF structure than reported before (i.e., high intermittency) which differs from the mostly monofractal structure of several commonly used simulated networks. We also point out that the MF properties of width and area functions are different, possibly reflecting the difference between the hillslope and channelized drainage patterns and begging further study.

[9] This paper is structured as follows. Section 2 presents a review of theoretical branching trees commonly used in hydrology and describes models for their corresponding width and area functions. Section 3 presents a concise overview of MF formalisms which includes the commonly used box aggregation and structure function methods but goes beyond with the use of wavelet-based methodologies. It also presents the cumulant analysis method for accurate estimation of the singularity spectrum parameters especially for short signals as those available for geomorphologic analysis. Section 4 presents a robust framework for MF analysis of area and width functions and demonstrates that care must be exercised in selecting the proper multiresolution coefficients. Section 5 derives numerically the MF properties of the area function of stochastic self-similar

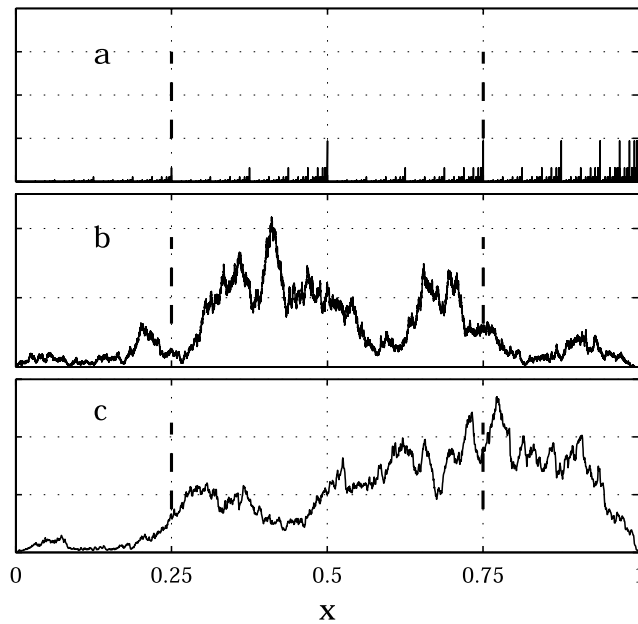


Figure 2. (a) Peano's basin, (b) Shreve's random network, and (c) stochastic self-similar model (with $(\alpha, \beta) = (1, 2)$) area functions. The corresponding order is $\omega = 18$ for Peano's basin and $\omega = 11$ for the stochastic self-similar model. The vertical dashed lines define the central half.

trees. Results from MF analysis are then presented and discussed for area and width functions of real river networks (section 6). Finally conclusions are given in section 7.

2. Models for Area and Width Functions of River Networks

2.1. Horton-Strahler Stream Ordering and Self-Similar Trees

[10] River network streams are usually classified according to the Horton-Strahler ordering scheme [Horton, 1945; Strahler, 1957]: the network is divided in links that connect either two tributary junctions (internal links) or a tributary junction and a channel source point (external links). (Note that for simplicity the definitions here are given for binary junctions but they can easily be extended to nonbinary ones.) Every external link is given order $\omega = 1$. One then applies a recursive algorithm to compute the order of every link: at every junction, two links of the same order ω give birth downstream to a link of order $\omega + 1$ while two links of order ω and ω' with $\omega \neq \omega'$ give birth downstream to a link of order $\max(\omega, \omega')$.

[11] Self-similar trees (SSTs) are topological descriptions of river networks first introduced by Tokunaga in 1966 and further studied by Tokunaga [1978] and Peckham [1995], among others. According to SSTs, every stream of order ω has two upstream tributaries of order $\omega - 1$ and several side tributaries of order ω' such that $1 \leq \omega' < \omega$. Let $T_{\omega, \omega'}$ denote the average number of tributaries of order ω' that branch into a stream of order ω . The assumption of self-similarity between streams (and associated drainage basins) of different orders [see, e.g., Rodríguez-Iturbe and Rinaldo, 1997] results in the constraint $T_{\omega, \omega'} = T_{\omega - \omega'} = T_k$ with $1 \leq k = \omega - \omega' \leq \omega - 1$. Tokunaga's trees [Tokunaga, 1978] are

trees for which the additional constraint holds $T_{k+1}/T_k = \text{const}$ which leads to a simple expression for T_k :

$$T_k = \alpha \cdot \beta^{k-1}. \quad (3)$$

This class of trees has been used to describe real river networks. For instance, Peckham [1995] successfully characterized a real river network with values $\alpha = 1.2$ and $\beta = 2.4$.

[12] Under the assumption that links are of constant length, it can be shown [Peckham, 1995] that the fractal dimension of such trees is

$$D = \frac{\log_2 \left[2 + \alpha + \beta + \sqrt{(2 + \alpha + \beta)^2 - 8\beta} \right] - 1}{\log_2 \beta}. \quad (4)$$

[13] This result is important since it defines a constraint on the choice of parameters α and β : one should choose these parameters such that $D < 2$ (non-space-filling network) or at most $D = 2$ (space-filling network). For instance $(\alpha, \beta) = (1, 2)$, which corresponds to Shreve's model to be discussed later, results in $D = 2$, i.e., a space-filling network.

2.2. Peano's Basin

[14] In a seminal work, Peano [1890] defined a fractal structure which has been widely used as a model of drainage networks, the so-called Peano's basin. Peano's basin defines a space-filling drainage network for which, as a result, the width and area functions coincide, i.e., $A(x) = W(x)$.

[15] Peano's basin is a specific case of the class of recursive replacement self-similar trees [see Peckham, 1995; Gupta and Waymire, 1996; Mandelbrot and Viscek, 1989] which is a subclass of the SSTs. The iterative building scheme of Peano's basin is illustrated in Figure 1. The tree at first step $\omega = 1$ consists of only one link of length 1. The tree at step ω is built from the tree at the previous order according to the following rule: each mother link of the network at step ω is replaced by four children links (whose lengths are the same and equal to half of the mother link), organized according to a cross pattern. The number of steps used for construction coincides with the largest stream order within the network and thus with the order of the network. This construction rule (which is purely deterministic) defines asymptotically a space-filling tree.

[16] The Peano's basin area function $A(x)$ can be easily derived and is shown to converge (when the number of iterations entering the Peano's basin construction tends to infinity) toward the Besicovitch's measure [e.g., Marani et al., 1991]. First, note that the distance x takes values in $[0, 1]$ for every order ω . The area function at step ω ($A(\omega; x)$) is related to that at the previous step $\omega - 1$ through

$$A(\omega; x) = \begin{cases} \frac{1}{4}A(\omega - 1; 2x) & \text{if } 0 \leq x < \frac{1}{2} \\ \frac{3}{4}A(\omega - 1; 2x - 1) & \text{if } \frac{1}{2} \leq x \leq 1 \end{cases} \quad (5)$$

and thus does coincide with the definition of Besicovitch's measure (or binomial measure) with parameter $p = \frac{1}{4}$. This last is the archetype for a MF measure (equivalently called

distribution) and its singularity spectrum $D(h)$ (see appendix for definition) can be easily derived and expressed with the parameterized formulas [see, e.g., *Schroeder*, 1991]

$$\begin{aligned} D &= -t \log_2 t - (1-t) \log_2 (1-t) \\ h &= -t \log_2 p - (1-t) \log_2 (1-p) \end{aligned} \quad (6)$$

with $0 < t < 1$ and $p = \frac{1}{4}$ for the specific case of Peano's basin.

[17] The Peano's basin model then predicts for the area function $A(x)$ a MF measure for which the singularity spectrum is known. The distribution $A(18; x)$ is plotted in Figure 2a and its MF analysis will be discussed in section 4.1.

2.3. Shreve's Random Topology Model

[18] *Shreve* [1966] introduced a stochastic model for river networks which provides also models for area and width functions. Shreve's model has been widely used to describe scaling properties of drainage networks and of their area and width functions [see, e.g., *Rodríguez-Iturbe and Rinaldo*, 1997; *Troutman and Karlinger*, 1984; *Agnese et al.*, 1998].

[19] Shreve's model is a binary branching tree defined through the very simple following construction rules. The main ingredient is the assumption that every link has equal probability to be either an exterior link (not connected to any other link upstream) or an interior link (connected to 2 links upstream). Construction of a realization of such a tree starts with one link. This link is then chosen with the same probability 0.5 to be an exterior link, and then the construction process ends, or an interior link and then 2 new children links are connected to it. The construction process recursively applies to each of the children links and so on until there are no more children links (i.e., all children links at previous steps have been chosen to be exterior links). The number of links of the Shreve's model is a random variable taking different values for every realization.

[20] The T_k coefficients can be computed for this model and are shown [see *Shreve*, 1966; *Tokunaga*, 1978; *Peckham*, 1995] to coincide with those of Tokunaga's SSTs: $T_k = \alpha \cdot \beta^{k-1}$ with specific values $(\alpha, \beta) = (1, 2)$.

[21] Shreve's random topology model defines a space-filling network [*Peckham*, 1995] and thus area and width functions coincide as for the Peano's model. $A(x) = W(x)$ is a stochastic process for which realizations can be generated using the following algorithm. $A(x)$ is indexed with an integer argument and is initially set as $A(1) = 1$. Then $A(x+1)$ is computed from $A(x)$ as $A(x+1) = \sum_{k=1}^{A(x)} y(k)$ where the $y(k)$ are independent and identically distributed random variables that take the values 0 or 2 with equal probability (i.e., probability 1/2). The construction algorithm ends when $A(x) = 0$. A realization with 109,270 samples is plotted in Figure 2b.

[22] The MF properties of the area function of Shreve's model can be roughly understood as follows. The increments of $A(x)$ can be written as

$$A(x+1) - A(x) = \sum_{k=1}^{A(x)} z(k), \quad (7)$$

where $z(k) = y(k) - 1$ are independent and identically distributed random variables that take the values $\{-1; 1\}$

with equal probability. The central limit theorem [see, e.g., *Feller*, 1966] states that the normalized sum of i.i.d. random variables with zero mean and unit standard deviation (that are thus finite), i.e., $\frac{1}{\sqrt{N}} \sum_{k=1}^N z(k)$, does converge (in the limit $N \rightarrow +\infty$) toward a random variable distributed with a normal law of zero mean and unit standard deviation. One may hence approximate $\sum_{k=1}^{A(x)} z(k)$ by a random variable distributed with a normal law with zero mean and standard deviation $\sqrt{A(x)}$, if $A(x)$ is "sufficiently" large. Then, the previous equation becomes

$$A(x+1) - A(x) \simeq \sqrt{A(x)} n(x), \quad (8)$$

where $n(x)$ is a Gaussian random variable with zero mean and unit variance. This last equation is a discrete version of the stochastic differential equation:

$$dA(x) = \sqrt{A(x)} dB(x) \quad (9)$$

where $B(x)$ is the ordinary Brownian motion. The Feller diffusion process is solution of this equation and $A(x)$ may thus be interpreted as a discrete version of the Feller diffusion process [see, e.g., *Etheridge*, 2000]. This last is a process whose realizations are functions (and not measures). This property may be easily understood since $A(x)$ is defined from a (discrete) differential equation. Moreover, the MF properties of the Feller diffusion are known: this process is monofractal, with Hölder exponent: $H = 0.5$ (*J. Beresticky*, University of Provence, Marseille, private communication, 2006).

[23] This last interpretation is clearly confirmed by numerical analysis of realizations of the process $A(x)$, as it will be shown in section 4.1.

2.4. Stochastic Self-Similar Trees and Their Area and Width Functions

[24] The following recursive algorithm is proposed to generate the area and width functions of SSTs. Note that every link is assumed to have the same length, which defines the unit length (i.e., every link has length 1).

[25] 1. The coefficients T_k are chosen to correspond to those of Tokunaga's trees: $T_k = \alpha \cdot \beta^{k-1}$.

[26] 2. Streams of order 1 possess only one link.

[27] 3. For every stream i of order ω , the number $X_k^{\omega,i}$ of side tributaries of order $\omega - k$ is chosen as the value taken by a random variable which is an integer and is distributed with a Poisson distribution with parameter $\lambda = T_k$. (Note that the mean of such a random variable is λ and its variance is also λ .) All the values $X_k^{\omega,i}$ are statistically independent; the choice of the $X_k^{\omega,i}$ then fixes the number of side tributaries of the stream i to $\sum_{k=1}^{\omega-1} X_k^{\omega,i}$ and hence its number of links to $C^{\omega,i} = 1 + \sum_{k=1}^{\omega-1} X_k^{\omega,i}$.

[28] 4. The locations of the junctions of every side tributary to the stream i are randomly and independently chosen, with a uniform distribution; that is, the probability of a given side tributary to link the stream i at the end of one of the $\sum_{k=1}^{\omega-1} X_k^{\omega,i}$ links is the same for every link and independent of the location of other side tributary junctions.

[29] 5. Two things are noted. First, a different choice for T_k coefficients than stated above can be used for the generation of area and width functions although this is not explored in this paper. Second, a specific choice of T_k does

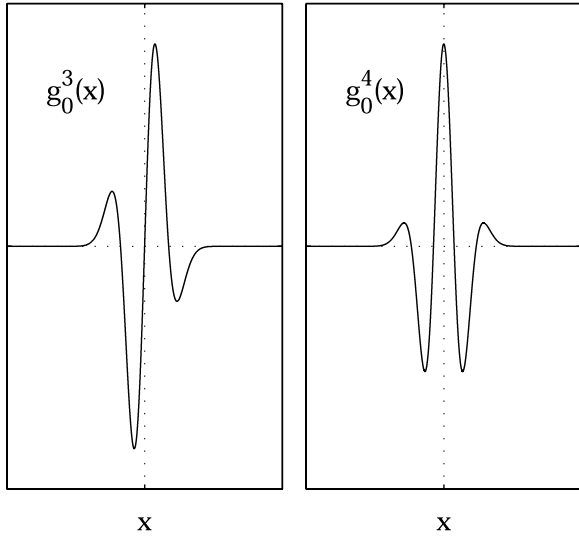


Figure 3. (left) Wavelets g_0^3 and (right) g_0^4 (arbitrary units).

not suffice in defining a unique model for width or area functions as will be demonstrated in section 5. This can be easily understood since the T_k are only the means of the distributions of the side tributaries and thus do not fully characterize them.

[30] 6. It is noted that the SSTs generated by the above algorithm form a specific case of the more general stochastic Tokunaga trees introduced by *Cui et al.* [1999]. The MF properties of the stochastic SSTs are not analytically derivable and will be studied via simulation in section 5.

3. Multifractal Analysis

3.1. Practical Multifractal Analysis

[31] MF formalisms aim to perform on actual data a MF analysis, i.e., estimate the singularity spectrum $D(h)$ (see Appendix A) from the statistics of the local fluctuations of the signal at different scales a and different locations x_0 . Let us denote these fluctuations, also called multiresolution coefficients, $c(x_0, a)$, and define the partition functions $S(q, a)$ as estimates (by space averaging) of their q th statistical moments:

$$S(q, a) = \frac{1}{n(a)} \sum_{x_0} |c(x_0, a)|^q, \quad (10)$$

where $n(a)$ is the number of coefficients $c(x_0, a)$ available at scale a . The scale invariance property of a signal results in power law behavior for the partition functions:

$$S(q, a) \sim a^{\tau(q)}, \quad (11)$$

defining the usual spectrum of scaling exponents $\tau(q)$, indexed by moment order q . The MF formalism eventually states that the scaling exponents relate to the singularity spectrum through a Legendre transform:

$$D(h) = \begin{cases} 1 + \min_q [qh - \tau(q)] & \text{for functions} \\ 1 + \min_q [qh - (q + \tau(q))] & \text{for measures.} \end{cases} \quad (12)$$

It is noted that the difference in the definitions of Legendre transform for functions and measures (see Appendix A for definition of a measure) is due to the common choice for normalization of the multiresolution coefficients (indeed, if one uses $a.c(x_0, a)$ instead of $c(x_0, a)$, the scaling exponents $\tau(q)$ are shifted to $q + \tau(q)$).

[32] Note that if the signal under analysis is monofractal then the scaling exponents vary linearly with respect to the moment order q , i.e., $\tau(q) = qH$. In contrast, if the singularity spectrum takes finite values on an interval $[h_{\min}, h_{\max}]$ with $h_{\max} > h_{\min}$, the scaling exponents $\tau(q)$ no longer define a linear but rather a nonlinear function.

3.2. Multiresolution Coefficients

[33] As discussed in the previous section one first needs to compute the multiresolution coefficients $c(x_0, a)$ in order to perform a MF analysis. There are several choices of multiresolution coefficients, that can be valid or not depending on the nature of the data under analysis, e.g., function or measure and the presence of nonstationarities. The correct selection of multiresolution coefficients is thus of first importance in order to perform a meaningful MF analysis.

3.2.1. Catalog of Multiresolution Coefficients

[34] The MF formalism was historically introduced with partition functions computed with first-order increments for functions (the so-called structure function method [*Parisi and Frisch*, 1985])

$$c(x_0, a) = \delta(x_0, a) = s(x_0 + a) - s(x_0) \quad (13)$$

and box aggregation coefficients for measures [*Hasley et al.*, 1986]

$$c(x_0, a) = b(x_0, a) = \frac{1}{a} \int_{x_0 - a/2}^{x_0 + a/2} s(x) dx. \quad (14)$$

Wavelet coefficients [*Mallat*, 1998] provide a more versatile and efficient choice for multiresolution coefficients and can be used for MF analysis of both functions and measures and for nonstationary signals [*Arneodo et al.*, 1995; *Jaffard*, 1997] (see also discussion below). Wavelet coefficients $w(x_0, a)$ are defined as the inner product between the data $s(x)$ and the wavelet $\psi_{x_0, a}(x)$, associated with location x_0 and scale a :

$$c(x_0, a) = w(x_0, a) = \int_{\mathbb{R}} \psi_{x_0, a}(x) s(x) dx, \quad (15)$$

where $\psi_{x_0, a}(x)$ is a scale-dilated and time-shifted template of the mother wavelet $\psi_0(x)$:

$$\psi_{x_0, a}(x) = \frac{1}{a} \psi_0\left(\frac{x - x_0}{a}\right). \quad (16)$$

[35] A commonly used wavelet family is the Gaussian wavelets (which are continuous wavelets; that is, spatial location x_0 and scale a can take on any real value), defined as the N -order derivative of a Gaussian function, modulus a proper multiplicative factor to ensure correct normalization. The derivative of order N is denoted as $g_0^N(x)$. Wavelets $g_0^3(x)$ and $g_0^4(x)$ are plotted in Figure 3.

[36] An important feature of the mother wavelet ψ_0 for practical purposes is its number of vanishing moments: $N \geq 1$ such that $\int x^k \psi_0(x) dx = 0$ if $0 \leq k \leq N - 1$ and $\int x^N \psi_0(x) dx \neq 0$. The use of a wavelet with a given N allows the removal of an additive polynomial trend of degree less than N (which can cause a failure of MF analysis [see *Arneodo et al.*, 1995]). From a practical point of view, the number of vanishing moments has to be chosen sufficiently high such that robustness of the results is achieved; that is, there is no dependence on the chosen wavelet. The Gaussian wavelet $g_0^N(x)$ can be easily shown to have N vanishing moments.

3.2.2. Choice of Multiresolution Coefficients

[37] The previous section depicts several choices of multiresolution coefficients: increments or wavelet coefficients for MF analysis of functions (including functions with polynomial trends) and box aggregation coefficients or wavelet coefficients for MF analysis of measures. The ability of wavelet coefficients to be used for analysis of both functions and measures can be understood qualitatively since a wavelet gathers local average and differentiation patterns (cf. Figure 3): the wavelet coefficients are thus a common extension of both increments and box aggregation coefficients. This assertion will be quantitatively illustrated in section 4.1 via an example.

[38] It is important to point out that an erroneous choice, such as the use of increments for a measure or the use of box aggregation coefficients for a function, or use of increments of insufficient order for a nonstationary signal, leads to artifacts and thus to misleading conclusions: a correct MF analysis requires a correct choice of multiresolution coefficients. Since often one does not know before hand the exact nature of the analyzed signal, a robust MF analysis framework is proposed in this paper (see section 4) which can both identify the correct mathematical nature of a signal (measure, function, degree of nonstationarity) and correctly estimate its singularity spectrum.

3.2.3. Moments of Negative Order q

[39] From the Legendre transform relationship (equation (12)), it is seen that

$$q = dD(h)/dh, \quad (17)$$

and thus for estimating the decreasing (right) part of the $D(h)$ function, in order to gain access to the whole range of singularities from h_{\min} to h_{\max} , one needs to consider estimation of $\tau(q)$ for negative moments q . The MF formalism based on increments, or even on continuous wavelet transform (CWT) coefficients $c(x_0, a)$, suffers from the fact that it is not valid for estimation of $\tau(q)$ for $q < 0$. This is because the probability distribution of increments or CWT coefficients is centered at zero and thus negative moments diverge [see, e.g., *Venugopal et al.*, 2006b]. This drawback can be overcome by using the WTMM (Wavelet Transform Modulus Maxima) methodology which operates on the modula of the wavelet coefficients which are always positive [*Muzy et al.*, 1993, 1994; *Arneodo et al.*, 1995]. This methodology defines the WTMM coefficients, denoted as $m(x_0, a)$, which can be used to compute the partition functions and thus the scaling exponents and the singularity spectra of functions. The reader is referred to *Muzy et al.* [1993, 1994], *Arneodo et al.* [1995], or *Venugopal et al.*

[2006a, 2006b] for detailed presentation and illustration of this MF formalism. It is also noted that a new MF formalism, relying on a well-defined mathematical basis and based on the so-called wavelet leaders (defined from the discrete wavelet transform [*Mallat*, 1998]) has been recently introduced in order to overcome this difficulty [*Jaffard et al.*, 2005; *Lashermes*, 2005; B. Lashermes et al., Wavelet leaders based multifractal formalism: A comprehensive analysis of turbulent velocity, submitted to *European Physical Journal B*, 2007].

3.3. Multifractal Parameter Estimation With Cumulant Analysis

[40] The scaling exponent function $\tau(q)$ reflects the MF properties of the data under analysis since it is the Legendre transform of the singularity spectrum $D(h)$. As discussed above, estimation of $\tau(q)$ typically relies on computation of the partition function $S(q, a)$ for different order moments q (equation (10)) and estimation of the slopes of the log-log linear plots of $S(q, a)$ versus scale a . In order to depict the deviation of $\tau(q)$ from linearity (the hallmark of multifractality) one has to estimate moments of high-order (the literature reports moments up to order $q = 10$). This presents not only problems of statistical convergence for short signals but also problems of interpretation of high moments due to a degenerate linear behavior of $\tau(q)$, theoretically expected for $q > q_{\max}$, where q_{\max} depends on the inherent MF nature of the analyzed signal. Basically, the maximum interpretable q is determined by the largest Holder exponent h_{\max} present in the signal; for $q > q_{\max}$ a linear $\tau(q)$ curve is expected even for a true MF signal. The reader is referred to *Lashermes et al.* [2004] and also *Venugopal et al.* [2006a] for further details on these estimation problems.

[41] An alternative estimation methodology, called cumulant analysis method, which avoids the need to compute high-order moments and also leads to a concise MF parameterization, has recently been introduced in the literature [e.g., *Arneodo et al.*, 1998; *Malécot et al.*, 2000; *Delour et al.*, 2001] and has been used in geophysics for the analysis of high-resolution temporal rainfall [*Venugopal et al.*, 2006a, 2006b]. The reader is referred to these publications for details on the methodology.

[42] The cumulant analysis method, provides an estimation of the parameters c_p of the Taylor series expansion of $\tau(q)$ for $q \rightarrow 0$:

$$\tau(q) = \sum_{p \geq 1} (-1)^{p-1} \frac{c_p}{p!} q^p \quad (18)$$

by computing the statistical cumulants $C(p, a)$ of order p of the logarithm of the absolute value of the multiresolution coefficients $c(x_0, a)$ at a given scale a . Similarly to the partition functions (cf. equation (10)), the cumulants define a function of p and a which is furthermore linear with respect to $\ln a$ for MF functions. For instance, for $p = 1$ and 2,

$$C(1, a) = \frac{1}{n(a)} \sum_{x_0} \ln |c(x_0, a)| \simeq a_1 + c_1 \ln a \quad (19)$$

$$C(2, a) = \frac{1}{n(a)} \sum_{x_0} [\ln |c(x_0, a)| - C(1, a)]^2 \simeq a_2 - c_2 \ln a. \quad (20)$$

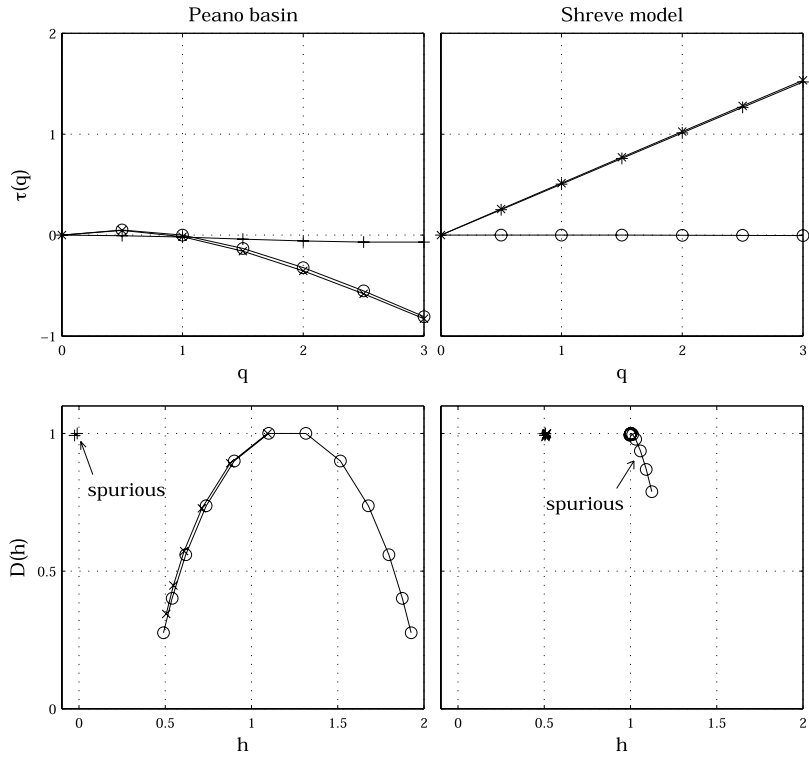


Figure 4. Measure or function? (top) Scaling exponents $\tau(q)$ and (bottom) predicted singularity spectra $D(h)$ computed with box aggregation (circles), increments (pluses), and wavelet coefficients (crosses) for (left) Peano’s basin and (right) Shreve’s model area function $A(x)$ (wavelet g_0^4). Scaling exponents are computed for negative q values for box aggregation coefficients in order to provide the right lobes of the singularity spectra; negative moments cannot be computed for increments or wavelet coefficients (see text for discussion).

Linear regressions of $C(p, a)$ versus $\ln a$ thus allow estimation of the c_p .

[43] If the process under analysis is monofractal then $c_1 = H \neq 0$ and $c_p = 0$ for $p > 1$. A nonzero value for c_2 explicitly establishes the multifractal (versus monofractal) nature of the data: c_1 is the most prevailing Hölder exponent value ($D(h)$ is maximum at $h = c_1$) and the parameter c_2 (also called the intermittency coefficient) relates to the spread of $D(h)$ around c_1 . The quadratic approximation of the scaling exponent function

$$\tau(q) \simeq c_1 q - c_2 q^2 / 2, \quad \text{when } q \rightarrow 0, \quad (21)$$

which corresponds to a quadratic approximation of the singularity spectrum,

$$D(h) \simeq 1 - \frac{(h - c_1)^2}{2c_2}, \quad \text{when } h \rightarrow c_1 \quad (22)$$

is a commonly used model of multifractality. This model has been shown to be both meaningful and a good approximation in turbulence (for which it corresponds to the so-called lognormal model).

[44] These tools will be applied in the sequel to characterize the MF properties of the width and area functions, using the CWT and the WTMM multiresolution coefficients. Since the WTMM coefficients allow the scaling exponent estimation both for $q < 0$ and $q > 0$, in contrast

to CWT coefficients which only allow estimation for $q > 0$, they are known to provide better estimators (faster statistical convergence for instance) at least for $p \geq 2$. The reader is referred to *Delour et al.* [2001] and *Venugopal et al.* [2006b] for further details of the methodology.

4. Potential Pitfalls and a Robust Methodology for Multifractal Analysis of Width and Area Functions

4.1. Discrimination Between Function and Measure: Peano’s Versus Shreve’s Models

[45] As was shown in section 2, different network topologies result in area and width functions that are distinctly different in terms of their mathematical nature. For example, the Peano basin area function is a mathematical measure (distribution) while that of Shreve’s model is a mathematical function. Analyzing both signals with the same multiresolution coefficients for estimating their singularity spectra, e.g., using for both the first-order structure function approach or the box-counting approach, can lead to misleading interpretations. The purpose of this section is (1) to quantitatively demonstrate that erroneous results on MF characterization can be obtained by an inappropriate choice of the multiresolution coefficients and (2) to present a framework for MF analysis which does not require a priori knowledge of the mathematical nature of the signal, but

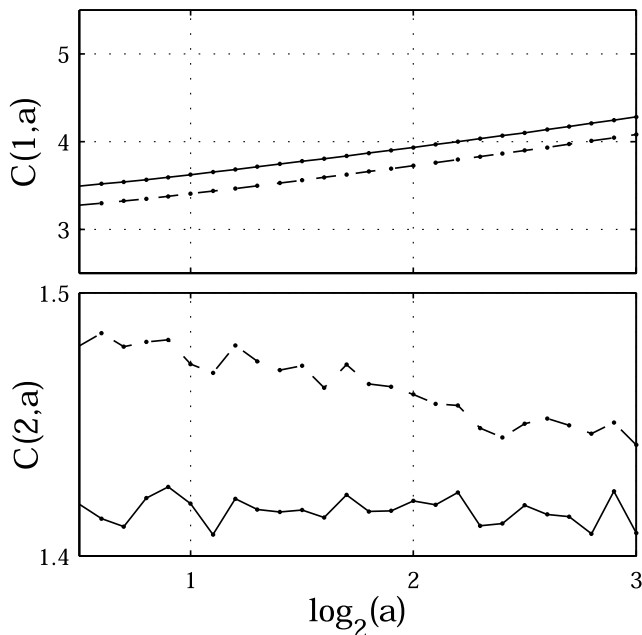


Figure 5. Effect of nonstationarity: average over $N = 100$ realizations of Shreve’s model area function of (top) first and (bottom) second cumulants of the whole realization (dashed line) and the central half (solid line) computed with CWT coefficients (wavelet g_0^4).

rather the framework identifies the underlying structure and selects the appropriate multiresolution coefficients.

[46] Let us denote the scaling exponent function $\tau(q)$ defined with box aggregation, first-order increments and wavelet coefficients, respectively, as $\tau^b(q)$, $\tau^\delta(q)$ and $\tau^w(q)$. We will demonstrate below that when all of them are computed from a sampled signal (data set), if $\tau^b(q)$ and $\tau^w(q)$ coincide and depart from $\tau^\delta(q)$, then the data under analysis correspond to a measure, whereas if $\tau^\delta(q)$ and $\tau^w(q)$ coincide and depart from $\tau^b(q)$, then the data under analysis correspond to a function

$$\begin{aligned} \tau^\delta(q) \neq \tau^w(q) = \tau^b(q) &\longrightarrow \text{measure} \\ \tau^\delta(q) = \tau^w(q) \neq \tau^b(q) &\longrightarrow \text{function.} \end{aligned} \quad (23)$$

[47] Moreover, if the interest is not really in inferring the mathematical nature of the signal but in correctly estimating its MF spectrum, the above framework depicts the appropriate multiresolution coefficients and leads to a correct estimate of the MF spectrum.

[48] MF analysis of the Peano’s and Shreve’s models area functions (cf. section 2) are performed using box aggregation, increment and wavelet coefficients (the wavelet used is g_0^4) and the results are shown in Figure 4. Scaling exponents

with negative q values are computed with box aggregated coefficients only, thus yielding the right lobe of singularity spectrum, since negative moments are statistically meaningless for increment or wavelet coefficients. As theoretically expected, the Peano model results in a (multifractal) measure for $A(x)$ and one observes $\tau^\delta(q) \neq \tau^w(q) \simeq \tau^b(q)$, whereas the Shreve model results in a (monofractal) function for $A(x)$ and one observes $\tau^\delta(q) \simeq \tau^w(q) \neq \tau^b(q)$. These results clearly show how to characterize the intrinsic mathematical nature of the digital (sampled) data under analysis without apriori information about the signal.

[49] Figure 4 illustrates as well the fact that an erroneous choice of multiresolution coefficients leads to an incorrect estimate of the spectrum of singularities. For instance, performing MF analysis of the function $A(x)$ predicted by the Shreve’s model using box aggregation coefficients (see Figure 4, right plots) leads to the erroneous conclusion that the singularity spectrum $D(h)$ (in the measure regularity sense) is reduced to one point with coordinates $(h = 1, D = 1)$ with a decreasing right lobe. However, using first-order increment and wavelet coefficients gives results in perfect agreement with the expectation discussed in section 2, i.e., $\tau^\delta(q) \simeq \tau^w(q) \simeq 0.5q$ which is indeed the Legendre transform of the singularity spectrum of a monofractal process with $H = 0.5$. As will be discussed below such analyses, i.e., using box aggregation coefficients for real network width functions, are commonplace in the literature and have resulted in suggestions that real networks have area functions with $D(h) = 1$ at $h \simeq 1$.

4.2. Nonstationarity Property of Area and Width Functions

[50] The area and width functions by definition start and end at zero. Moreover, if the length of the longest flow path is L , few pixels or links are located close to the basin outlet (i.e., at flow distance $x \ll L$) or at distance close to L (i.e., at flow distance x such that $(L - x) \ll L$). These functions then exhibit a nonstationary behavior which one has to deal with before performing practical MF analysis. As discussed previously, the MF analysis indeed assumes a stationarity property for the local distribution of Hölder exponents: this last is expected to be everywhere the same, which allows to replace statistical averages by spatial averages for the estimation of moments defining the partition functions (cf. equation (10)). It is noted that although the wavelet-based MF formalism can automatically deal with nonstationary signals in terms of removing polynomial trends (since by using wavelets with N vanishing moments a polynomial of degree N is filtered out from the signal), the form of nonstationarity in the width and area functions is of a particular type arising from the fact that close to the outlet and the upper end of the river basin, the branching structure is not well developed yet and this is reflected in the

Table 1. Different Parameter Sets Investigated for Stochastic Self-Similar Model

(α, β)	(0.75, 1.894)	(1, 2)	(1.25, 2.095)	(1.5, 2.183)	(1.75, 2.266)	(1.5, 2.5)	(1, 3)
D	2	2	2	2	2	1.76	1.41
order	13	12	11	11	10	10	10
\bar{n}	3894	4160	3618	5817	3950	6435	14827

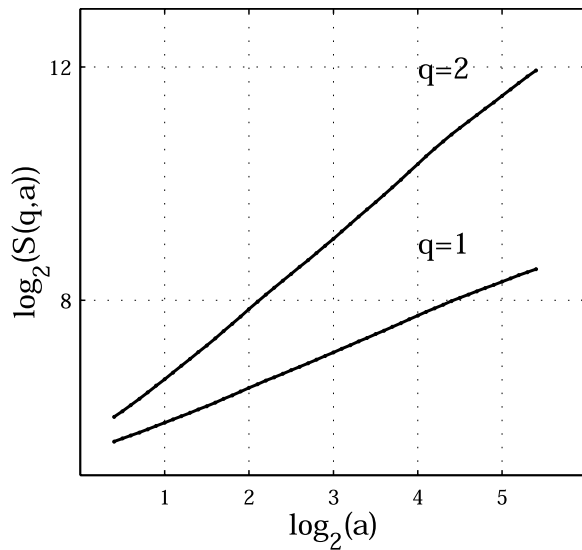


Figure 6. Stochastic self-similar model $((\alpha, \beta) = (1, 2))$ partition functions of order $q = 1, 2$ computed with CWT coefficients (wavelet g_0^4).

statistical nature of the width function fluctuations close to $x = 0$ and $x = L$.

[51] To assess the effectiveness of practical MF analysis to accurately estimate the MF spectra of the data under consideration, the analysis is performed both on the whole realization and on its central half only (i.e., if the realization has n samples, its central half is defined as the part between $n/4$ and $3n/4$) of the Shreve's model area function (cf. section 2.3). The results obtained with cumulant analysis are discussed below.

[52] Averages over 100 realizations (of length between 4096 and 8092 samples) of first and second-order cumulants (computed with CWT coefficients and wavelet g_0^4) for both the whole realization and the central part are plotted in Figure 5. All cumulants exhibit power law behavior and the cumulant exponents can hence be estimated. Estimation of the first-order cumulant exponent results in $c_1 \simeq 0.53 \pm 0.02$ for the whole realization and $c_1 \simeq 0.49 \pm 0.03$ for the central half, both statistically consistent with the expected value $c_1 = 0.5$. However, it is obvious that for the case when the whole realization is used, $C(2, a)$ has a significantly different than zero slope ($c_2 > 0$) while when the central half only is used, $C(2, a)$ is constant ($c_2 \simeq 0$). Interpreting these results through a MF lens would lead to conclude a multifractality for the whole realization and monofractality for its central half. MF analysis on the whole realization is then misleading since the function $A(x)$ is known to be monofractal with $H = 0.5$.

[53] We then conclude that the data fluctuations within the central part of the width and area functions may be assumed to be stationary and that MF formalisms may be meaningfully applied to the central half giving results that correctly reflect the properties of the underlying branching structure of the network [see also Veneziano *et al.*, 1995]. MF analysis of area and width functions of all networks (either synthetic or real) discussed in this paper is then performed on the central half for the remaining of this paper.

4.3. Analysis of Real Width and Area Functions: A Review of Other Efforts

[54] Several studies have considered MF analysis of width and area functions of real and simulated river networks [e.g., Rinaldo *et al.*, 1993; Marani *et al.*, 1994; Veneziano *et al.*, 1995; Yang *et al.*, 2001; Richards-Pecou, 2002] but some of the findings need to be reconsidered. First, several studies have reported that the area function of real river networks is a multifractal with $D(h) = 1$ at $h \simeq 1$ and a slowly falling right limb for $h > 1$ [e.g., see Rodríguez-Iturbe and Rinaldo, 1997, Figures 3.16, 3.17, 3.23; Yang *et al.*, 2001]. The same results have been reported for simulated optimal channel networks (OCNs) [e.g., see Rodríguez-Iturbe and Rinaldo, 1997, Figures 4.26, 42.7].

[55] These studies have used the box-counting method, which works fine for the Peano basin whose $A(x)$ is a measure, but is not appropriate for the Shreve model or for real networks for which the $A(x)$ is a function. It is worth noting that an estimate of $D(h)$ concentrated around $h = 1$ has prompted suggestions in the literature that the width function of real networks is close to that of the Peano basin for which the theoretical H is 1.207. This is an artifact of the analysis methodologies.

[56] A second problem is that inferences about the deviation from multifractality (nonlinear $\tau(q)$) have been based on very high order moments (e.g., from -10 up to 10) computed from short series. This can lead to spurious lobes of the singularity spectrum. Yet, since the left lobe is always found to decrease very rapidly allowing thus no discrimination (e.g., see the previously mentioned figures in the literature), the right lobe has been used for discriminating among modeled and real networks and also for assessing the effects of threshold area for channel initiation on the MF properties of width functions [e.g., see Rodríguez-Iturbe and Rinaldo, 1997, Figure 3.23; Yang *et al.*, 2001]. This

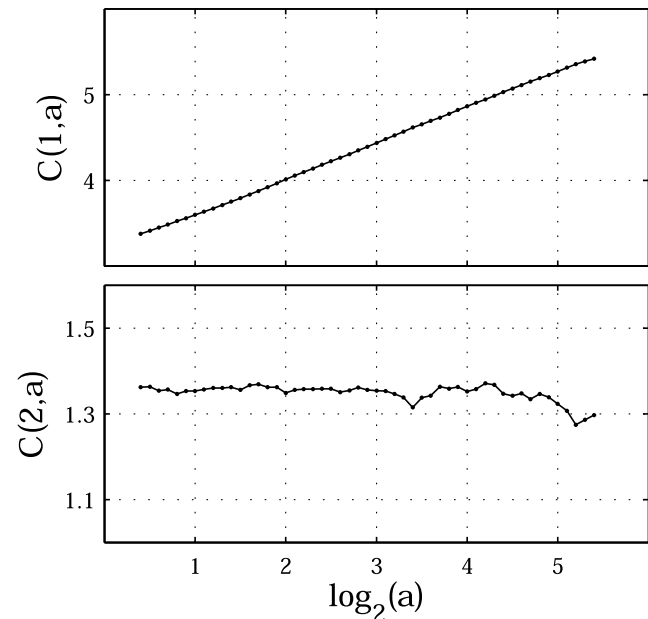


Figure 7. Stochastic self-similar model $((\alpha, \beta) = (1, 2))$ cumulants of order (top) $p = 1$ and (bottom) $p = 2$ computed with CWT coefficients (wavelet g_0^4).

Table 2. Mean of Cumulant Exponents for Area Functions of Stochastic Self-Similar Trees, Computed on the Central Half Portion With CWT and WTMM Coefficients Averaged Over $N = 100$ Realizations^a

	(α, β)	(0.75, 1.894)	(1, 2)	(1.25, 2.095)	(1.5, 2.183)	(1.75, 2.266)
CWT	c_1	0.65 ± 0.01	0.62 ± 0.01	0.55 ± 0.01	0.55 ± 0.01	0.55 ± 0.01
	c_2	0.00 ± 0.01	0.01 ± 0.01	0.00 ± 0.01	0.01 ± 0.01	0.00 ± 0.01
	c_3	0.00 ± 0.04	0.01 ± 0.02	0.01 ± 0.02	0.00 ± 0.02	-0.01 ± 0.04
WTMM	c_1	0.64 ± 0.02	0.60 ± 0.01	0.56 ± 0.01	0.56 ± 0.01	0.54 ± 0.01
	c_2	0.01 ± 0.01	0.00 ± 0.01	0.00 ± 0.01	0.00 ± 0.01	0.01 ± 0.01
	c_3	0.02 ± 0.01	0.00 ± 0.01	0.01 ± 0.01	0.01 ± 0.01	0.01 ± 0.01

^aThe wavelet used is g_0^4 . The given confidence intervals are $\pm 2\sigma / \sqrt{N}$, where σ is the estimated standard deviation. Note that all considered combinations of (α, β) parameters result in space-filling trees (see equation (4)).

right lobe however is all an artifact of the analysis methodology; it relies on negative statistical moments which, although statistically feasible to compute from box aggregation coefficients, have no meaning since the box aggregation coefficients are not appropriate for analyzing a MF function. The proposed framework (using WTMM coefficients and cumulant analysis) provides accurate estimates of the whole singularity spectrum and also a concise parameterization which does not require the computation of high-order moments.

5. Numerical Multifractal Characterization of Stochastic Self-Similar Trees

[57] The stochastic SSTs presented in section 2.4 do not receive analytical expressions for the MF properties of their area and width functions. Thus these properties are investigated through numerical analysis of a large number (100) of realizations with the same values for order ω and parameters α and β (cf. Table 1). Several values of the parameters (α, β) are investigated with practical MF analysis, corresponding both to space-filling or non-space-filling networks. Note that the network orders have been chosen so that the average number of samples, denoted as \bar{n} , is almost the same for every choice of parameters α and β .

[58] The first step is to check that both partition functions and cumulants do behave like power laws with respect to scale a . For (α, β) values corresponding to space-filling networks this is indeed true (cf. Figures 6 and 7 for $(\alpha, \beta) = (1, 2)$); similar power law behaviors are observed for other

parameter value choices) but no clear power law behavior is observed when the network is not space filling. The origin of the departing behavior from scaling is intriguing and requires further study in the future. Here, only (α, β) values such that $D = 2$ are considered, thus defining processes for which the practical MF analysis is fully consistent and results in reliable estimates of the scaling and cumulant exponents.

[59] MF analysis is performed on the central half of every realization, using both the CWT and WTMM methodology (the wavelet used is g_0^4). Table 2 presents the results obtained for the three first cumulant exponents. For every set of parameters (α, β) , the results obtained from the numerical analysis, within confidence intervals (confidence interval is the common 95% confidence interval for the empirical average estimator on N samples of a Gaussian random variable: $\pm 2\frac{\sigma}{\sqrt{N}}$ where σ is the estimated standard deviation), show a monofractal behavior, characterized by the parameter c_1 only. Moreover, the estimated value of c_1 depends on the choice of (α, β) and ranges from 0.54 to 0.65, which are all larger than the one corresponding to Shreve's model area function (i.e., 0.5). Also, it is interesting to note that for (α, β) corresponding to space-filling SSTs, c_1 clearly decreases when α increases. In other words, when the "branching rate," that is, the number of tributaries of streams of a given order increases, the area function exhibits wilder fluctuations and becomes more and more irregular.

[60] Another interesting result concerns the values obtained for $(\alpha, \beta) = (1, 2)$: though the T_k coefficients of the

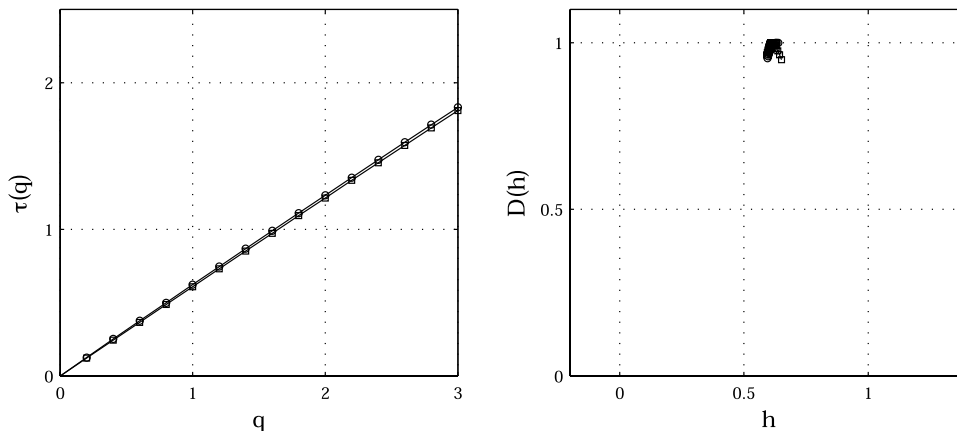


Figure 8. Stochastic self-similar model $((\alpha, \beta) = (1, 2))$ (left) scaling exponents $\tau(q)$ and (right) singularity spectrum $D(h)$ of area function $A(x)$ computed with CWT (circles) and WTMM (squares) coefficients (wavelet g_0^4).



Figure 9. Drainage basins and river networks for (top left) Walawe River (DEM resolution 90 m), Sri Lanka; (top right) South Fork Eel River (DEM resolution 1 m), California, United States; and (bottom) Noyo River (DEM resolution 10 m), California, United States.

underlying trees do coincide with those of the Shreve's model (cf. section 2.3), the related area functions clearly exhibit different regularity properties, i.e., with $H = 0.50$ for Shreve's model (see Figure 4, right) or $H = 0.60$ for SSTs (see Figure 8). This result supports the fact that knowledge of the coefficients T_k is not sufficient information to fully characterize a river network, since the T_k are only the means of the distributions of the number of side tributaries and do not account for higher-order statistical moments. A systematic analysis of the MF properties of the more general stochastic SSTs introduced by Cui *et al.* [1999], is an interesting topic for further study which however falls outside the scope of the present paper.

6. Multifractal Analysis of Real River Basin Area and Width Functions

6.1. Data Used for Analysis

[61] Analysis of area and width functions extracted from DEM of three real river basins (Figure 9) is performed in this paper. Walawe River is a river located in Sri Lanka and its drainage area is almost 2000 km². The area ($A(x)$) and width ($W(x)$) functions are extracted from DEM of spatial resolution 90 m \times 90 m. The area function of the upper part of the South Fork Eel River basin, California, USA (corresponding drainage area of 154 km²) is extracted from high-resolution 1 m \times 1 m DEM (LIDAR technology) and 10 m \times 10 m DEM (see Gangodagamage *et al.* [2007] for more details on this basin). Finally, the area and width function of the Noyo River basin, California, USA are

extracted from DEM of spatial resolution 10 m \times 10 m (corresponding drainage area of 143 km² [see Sklar *et al.*, 2006, and references therein] for more details on this basin). All these basins are plotted in Figure 9.

[62] From a practical point of view, one important parameter when extracting the area and width functions from a DEM is the bin size dx : $\{A(dx; x)\} = \# \{all M: x \leq l(M) \leq x + dx\}$, where $l(M)$ denotes the flow distance of pixel M to the outlet. One should carefully select the value for dx : if dx is too close to the DEM spatial resolution, then the computed $A(x)$ or $W(x)$ will take only small integer values and thus will be polluted by high-digitization noise. This effect can be specifically important for $W(x)$ since the percentage of channelized pixels is very small. On the other hand, a large value for dx may mask, because of averaging, the MF signatures of the underlying network structure. The bin size dx is chosen sufficiently large so as not to affect the results presented in this paper. The number of samples is 2,513 for the Walawe River area and width functions, 3,962 for the South Fork Eel River area function and 1,948 for the Noyo River area and width functions. All area and width functions are plotted in Figure 10.

6.2. Multifractal Characteristics of Several River Basin Area Functions

[63] The singularity spectra of the area and width functions of the Walawe river basin have been computed using box aggregation, increment and wavelet coefficients (the wavelet used in this section is g_0^4).

[64] The results are plotted in Figure 11 in a similar way as for the synthetic data (see Figure 4). Both for area and

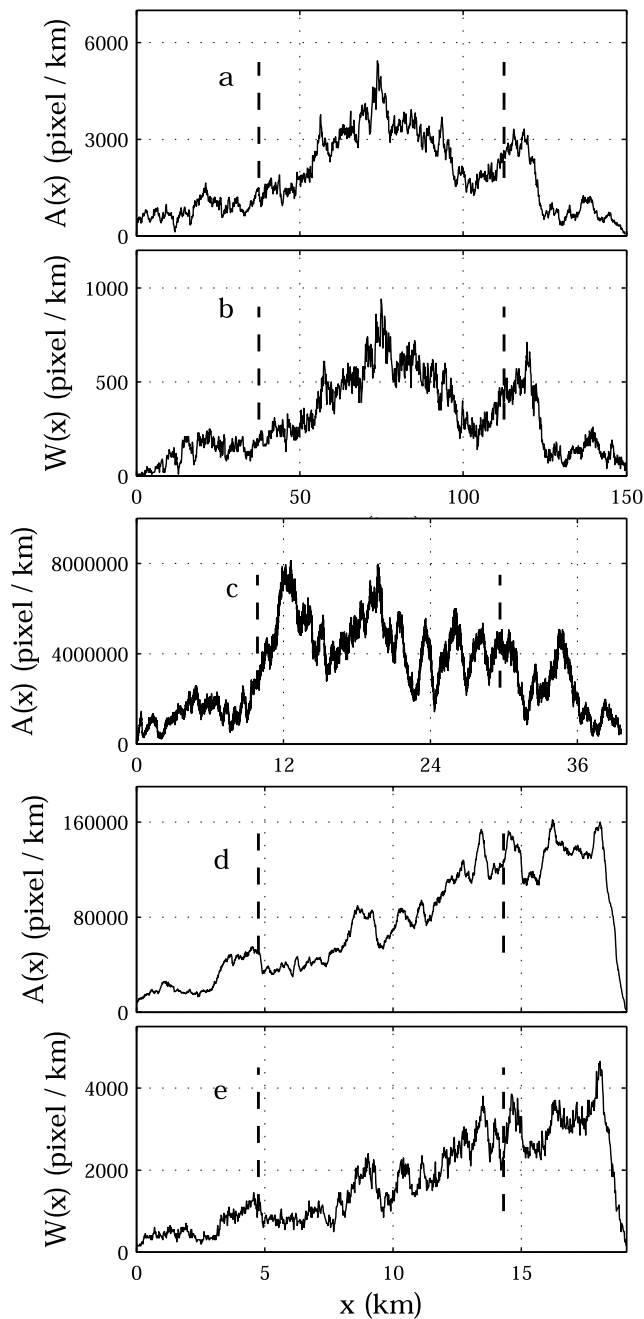


Figure 10. Area and width functions for Walawe River basin (a) area and (b) width functions, South Fork Eel River basin (c) area functions, and Noyo River basin (d) area and (e) width functions. The vertical dashed lines define the central half portion of the signal on which the MF analysis was performed.

width functions an agreement between the scaling exponents computed with increments and wavelet coefficients is found: $\tau^\delta(q) \simeq \tau^w(q)$, whereas the scaling exponents computed with box-aggregated coefficients $\tau^b(q)$ clearly depart from $\tau^\delta(q) \simeq \tau^w(q)$. We then conclude that both the area and width functions extracted from the Walawe River basin are by nature functions and not measures. The same result is obtained for the area function of the South Fork Eel River and Noyo River basins. Furthermore, as it is seen in

Figure 11 using box aggregation coefficients results in the wrong inference of MF properties close to those of Shreve's model as previously reported in the literature (cf. Figure 4), i.e., one point with coordinates ($h \simeq 1$, $D = 1$) with a decreasing right lobe, while using the increments or wavelet coefficients results in singularity spectrum centered at c_1 approximately 0.4 for $A(x)$ and 0.5 for $W(x)$.

[65] Figures 12 shows the log-log plots of the partition functions $S(q, a)$ versus a for $q = 1, 2$ computed using CWT and WTMM coefficients for the three different basins. The range of scales over which linear fits of the $\log_2(S(q, a))$ versus $\log_2(a)$ plots have been performed is shown in Table 3. On the basis of these fits, the $\tau(q)$ and (via the Legendre transform) $D(h)$ spectra were estimated and are shown for all three basins in Figure 13.

[66] Cumulant analysis for estimation of the parameters c_p has also been performed for all these basins using the CWT and WTMM coefficients. For illustration purposes, Figure 14 shows the cumulants $C(p, a)$ versus $\log a$ for $p = 1, 2$ for the Walawe basin; similar plots were found for the other basins. Using the range of scales reported in Table 3, the estimates of c_1 and c_2 were computed and are reported in Table 4. It is observed that the singularity spectra of the area functions of the three analyzed basins are clearly different as are the estimates of their c_1 and c_2 coefficients. More precisely, the singularity spectra of South Fork Eel River and Noyo River basins have their peak at $h = c_1 \simeq 0.8$ which is significantly larger than the value around which the peak of the singularity spectrum of the Walawe River basin is found: $h = c_1 \simeq 0.4$. It is moreover worth noting that the numerical analysis performed on both 1 m and 10 m resolution data sets (South Fork Eel River) yield the same results (cf. Table 4) supporting the fact that the observed difference in the value of c_1 is not an artifact due to the fine 1 m spatial resolution.

[67] The observed differences in the estimated values of the parameter c_1 means that the South Fork Eel River and Noyo River basins area functions exhibit more regular (in terms of singularity, i.e., larger c_1) local behavior than the Walawe River one. Eventually, all these area functions are MF functions, characterized by values of the parameter c_2 around 0.05 to 0.11. These values can be compared to the well known value of $c_2 \simeq 0.025$ for Eulerian turbulent velocity [e.g., Frisch, 1995] and values $c_2 \simeq 0.30$ for fine resolution (seconds) temporal rainfall [e.g., Venugopal *et al.*, 2006a].

[68] The robustness of the estimation methods used in this work enables us to confidently conclude that indeed there are significant differences in the singularity spectra of $A(x)$ of different basins. This is an encouraging result and points to the possibility that differences in the geomorphological processes controlling flow paths, both on the river network itself and on the hillslopes, might be reflected in the scaling properties of the area and width functions. A comprehensive analysis of a large number of basins needs to be undertaken to systematically study these connections.

6.3. Comparison Between Area and Width Functions

[69] In this section, the MF properties of the width and area functions of the Walawe River and Noyo river basins are compared. The scaling properties of the width function of the South Fork Eel River basin could not be reliably

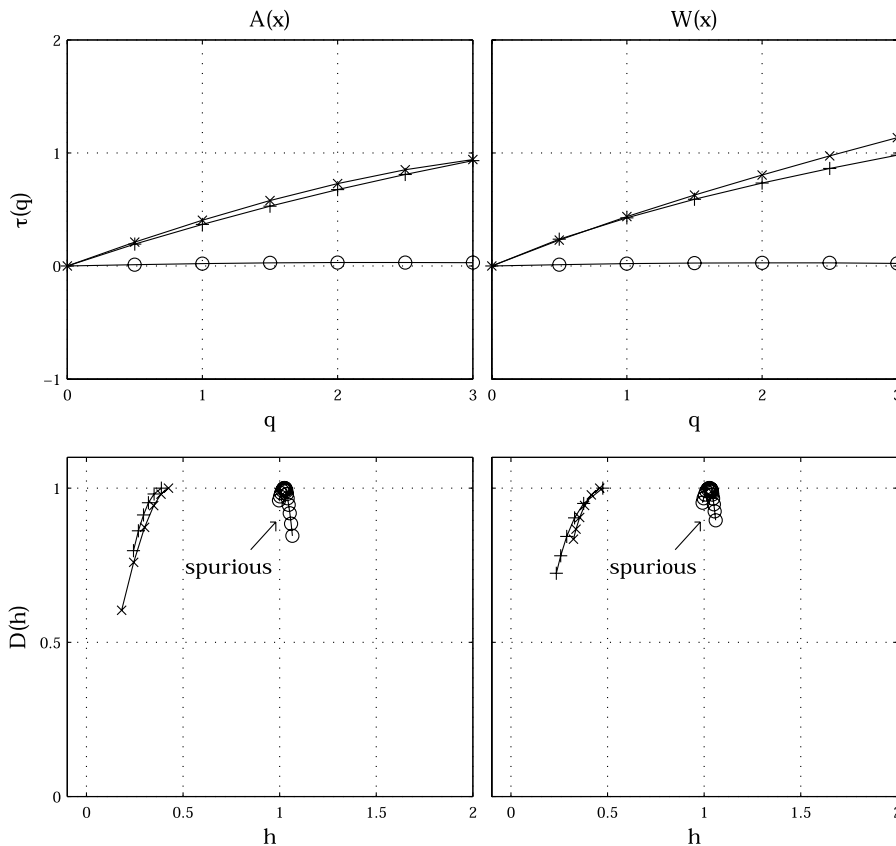


Figure 11. Walawe River (top) scaling exponents $\tau(q)$ and (bottom) predicted singularity spectra $D(h)$ computed with box-aggregation (circles), increments (pluses), and wavelet coefficients (crosses) for (left) area function $A(x)$ and (right) width function $W(x)$ (wavelet g_0^4). Scaling exponents are computed for negative q values for box aggregation coefficients in order to provide the right lobes of the singularity spectra; negative moments cannot be computed for increments and wavelet coefficients (see text for discussion).

analyzed because no sufficiently large scaling range was available for estimation.

[70] The scaling exponents $\tau(q)$ and the cumulant exponents c_p are computed from the CWT coefficients, using the wavelet g_0^4 . The results are reported in Figure 15 and Table 5. It is first important to note that the width function $W(x)$ cannot be analyzed using the WTMM coefficients as the scale range within which a power law behavior is observed for the partition functions defined from the CWT coefficients is quite small, and it is known that use of WTMM coefficients results in an even smaller scaling range (a larger value of a_{min}), making it hard to estimate the scaling or cumulant exponents.

[71] Figure 15 shows that the computed scaling exponents $\tau(q)$ and then the estimated singularity spectra $D(h)$ vary appreciably. This difference is quantified with the cumulant exponent c_1 since this is actually the abscissa of the maximum value of $D(h)$: $c_1 \simeq 0.5$ for $W(x)$ and $c_1 \simeq 0.4$ for $A(x)$ for the Walawe River basin, and $c_1 \simeq 0.5$ for $W(x)$ and $c_1 \simeq 0.8$ for $A(x)$ for the Noyo River basin (see summary in Table 5). It is worth noting that while the MF properties for $W(x)$ are similar for these two basins, $A(x)$ was found much “rougher” for the Noyo River basin and “smoother” for the Walawe River basin. The apparent “smoothness” of the hillslope dissection for the Walawe

River basin may simply be the result of the 90 m DEM resolution which is not enough to resolve the drainage patterns at the hillslope scale. This needs further study by a systematic analysis of several basins at high resolution and also by theoretical constructs in which distinctly different branching structures are superimposed on the basic branching structure of the river network. However, it is worth noting that both $A(x)$ and $W(x)$ are found MF (as opposed to monofractal) functions as their singularity spectra are not reduced to one point and c_2 is significantly different than zero.

7. Concluding Remarks

[72] The problem of extracting geomorphologic features from landscapes which allow distinct characterization and can be used for discrimination or classification purposes, has been of continuous interest in hydrogeomorphologic research. It is therefore of interest to examine whether the width and area functions of real basins imbed in them distinct signatures of landscape dissection which could be used to differentiate between different network or drainage path topologies. These distinct geomorphological features would also be expected to result in distinct hydrological behavior.

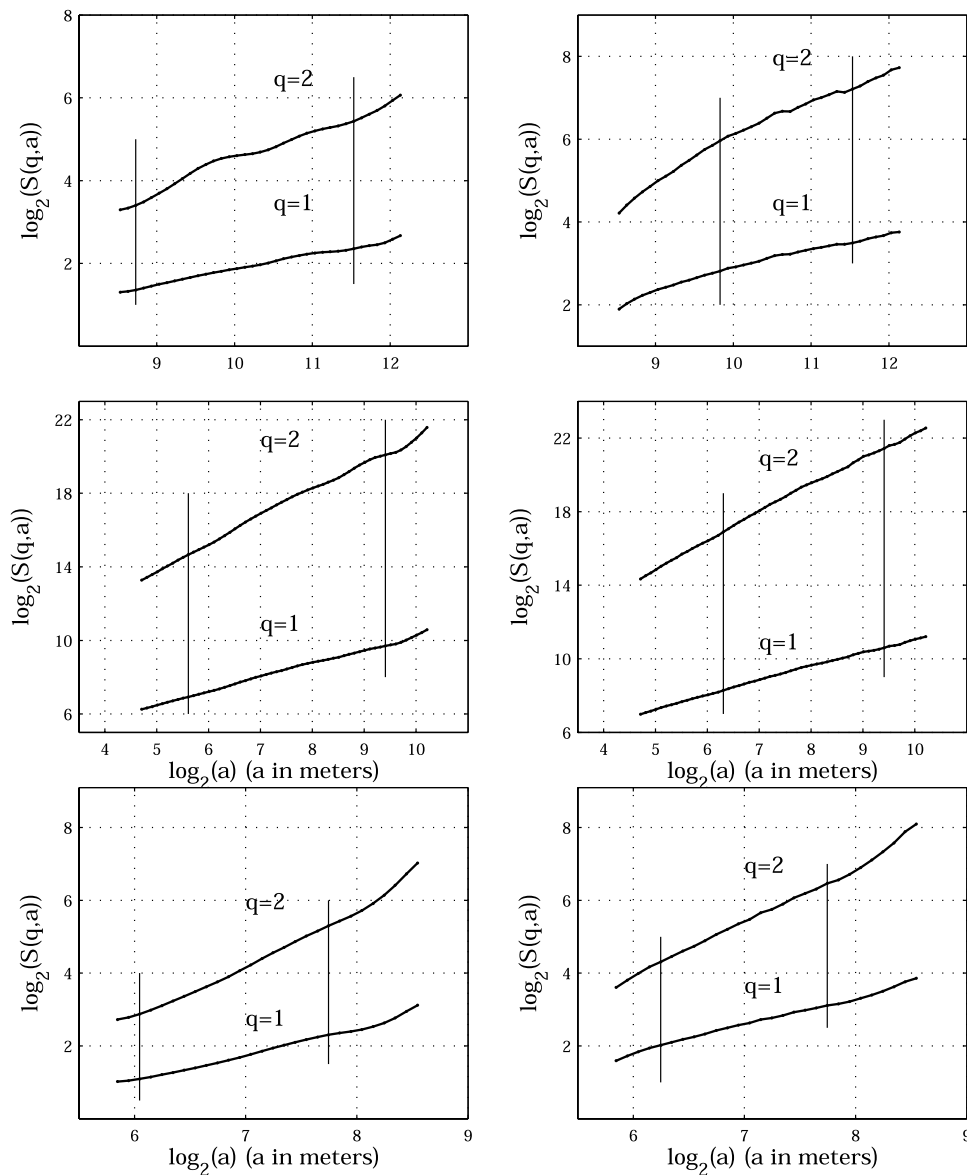


Figure 12. Partition functions of area functions $A(x)$: partition functions of order $q = 1, 2$ computed using (left) CWT and (right) WTMM coefficients for (top) the Walawe River basin, (middle) the South Fork Eel River basin, and (bottom) the Noyo River basin (wavelet g_0^4). Vertical lines denote the range of scales over which estimation of $\tau(q)$ is performed (see Table 3).

[73] In this paper we presented a robust framework for multifractal (MF) analysis of width and area functions of simulated and real river networks using wavelets. We pointed out the subtleties and potential pitfalls of such analyses, and introduced a new methodology, called cumulant analysis, for accurate and concise parameterization of multifractality using mainly two parameters, c_1 and c_2 : c_1 is the most frequently occurring singularity, and c_2 , the so-called intermittency coefficient, depicts the degree of deviation from monofractality and characterizes the degree of spatial heterogeneity of fluctuations. It is noted that for a monofractal, $c_1 = H$ and that a higher (lower) value of c_1 implies a “rougher” (“smoother”) signal.

[74] The results obtained in this work establish some trends but also highlight the need for further research along three main directions.

Table 3. Scale Ranges Used for Log-Log Linear Regressions of the Partition Functions^a

	Function	Method	a_{\min} , m	a_{\max} , m
Walawe River	$A(x)$	CWT	425	2960
		WTMM	911	2960
South Fork Eel R. (1 DEM)	$A(x)$	CWT	2400	5920
		WTMM	49	552
South Fork Eel R. (10 DEM)	$A(x)$	CWT	79	552
		WTMM	64	837
Noyo River	$A(x)$	CWT	112	837
		WTMM	66	429
	$W(x)$	CWT	76	429
		WTMM	132	697

^aSee Figure 12. Note that the same wavelet (g_0^4) has been used for all the analyses.

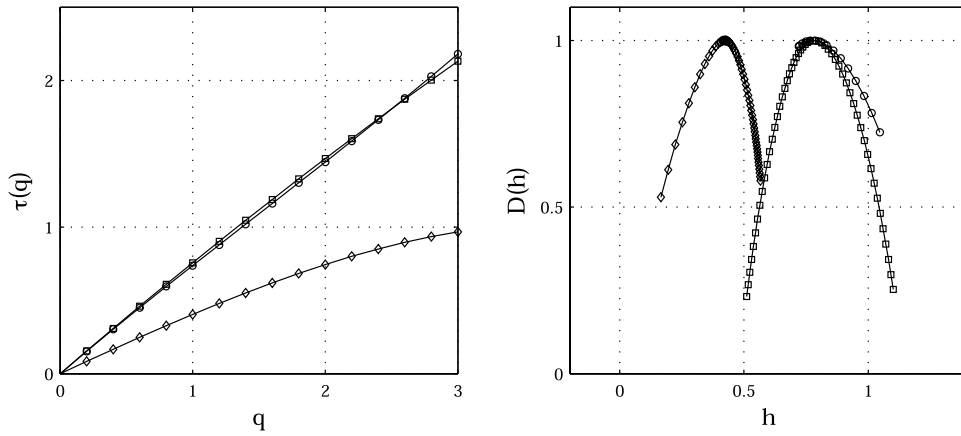


Figure 13. Area functions: (left) scaling exponents $\tau(q)$ and (right) singularity spectra $D(h)$ of Walawe River basin (diamonds), South Fork Eel River basin (squares), and the Noyo River basin (circles) area functions $A(x)$ (wavelet g_0^4).

7.1. Simulated Versus Real River Networks

[75] Our results established differences between the multi-scale statistical structure of area functions $A(x)$ of real networks (found to be multifractal, as opposed to monofractal, with c_1 between 0.4 to 0.8 and a considerable intermittency) and that of a large class of commonly used space-filling SSTs (found to be monofractal with H between 0.5 to 0.65). We also pointed out that previous studies that have inferred multifractality in real river networks with c_1 close to 1.0 suffer from artifacts of the analysis methodology. Given the increased use of simulated river networks in understanding the interplay between space-time precipitation variability and river network topology on the emergent scaling of floods, the proposed robust MF analysis frame-

work offers opportunity to study several new and relevant questions that have emerged from our analysis.

[76] 1. Do simulated self-similar trees (SSTs) which are not space-filling exhibit scaling in their width functions? Preliminary evidence in this paper suggests that scaling might not be present in these trees (see section 5) but this needs to be further investigated. This question is relevant as real river networks are not always space filling.

[77] 2. What class of SSTs exhibits multifractality in their width functions $W(x)$ similar to that exhibited by real river networks? One possible class is the extended class of stochastic SSTs proposed by Cui *et al.* [1999], which considers an additional source of spatial variability by randomizing the mean λ of the Poisson distribution of the number of side tributaries (see section 2.4). The MF properties of this extended class of models have not been studied yet, to the best of our knowledge. It is conjectured that this class might lead to width functions with multifractal (as opposed to monofractal) singularity spectra as those found in real networks and that this extra source of “randomness” might be a necessary condition for multifractality. This problem requires further study.

[78] 3. Do the MF parameters of $W(x)$ relate to any specific topological properties of the branching trees? In this study we found that for space-filling SSTs, a decreasing c_1 (rougher $W(x)$) corresponded to an increasing branching rate (see section 5). This implies that a “smoother” $W(x)$ might be expected for a branching network that has a smaller branching rate. Does this relation hold for other

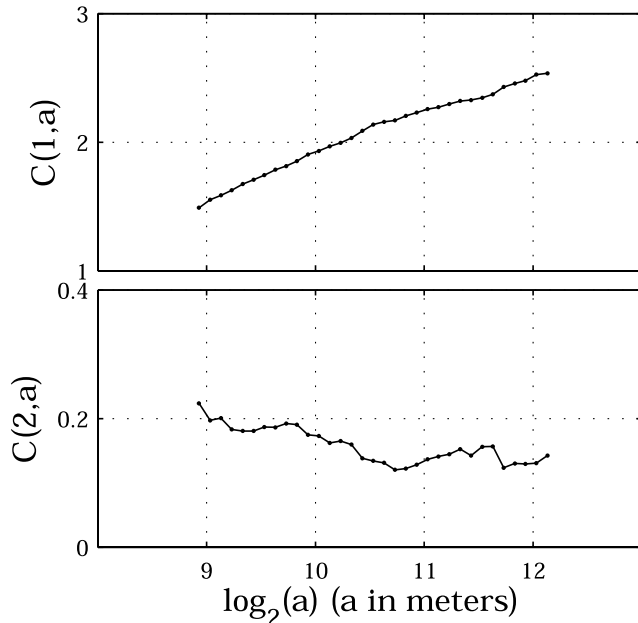


Figure 14. Walawe River cumulants of order $p = 1, 2$ of the area function $A(x)$ computed with WTMM coefficients (wavelet g_0^4).

Table 4. MF Characteristics of $A(x)$ for Several Basins^a

		South Fork Eel River			
		Walawe River	1 DEM	10 DEM	Noyo River
CWT	c_1	0.37	0.78	0.80	0.77
	c_2	0.06	0.05	0.05	0.11
WTMM	c_1	0.42	0.78	0.77	0.78
	c_2	0.03	0.06	0.04	0.10

^aCumulant exponents are computed with CWT and WTMM coefficients (wavelet g_0^4).

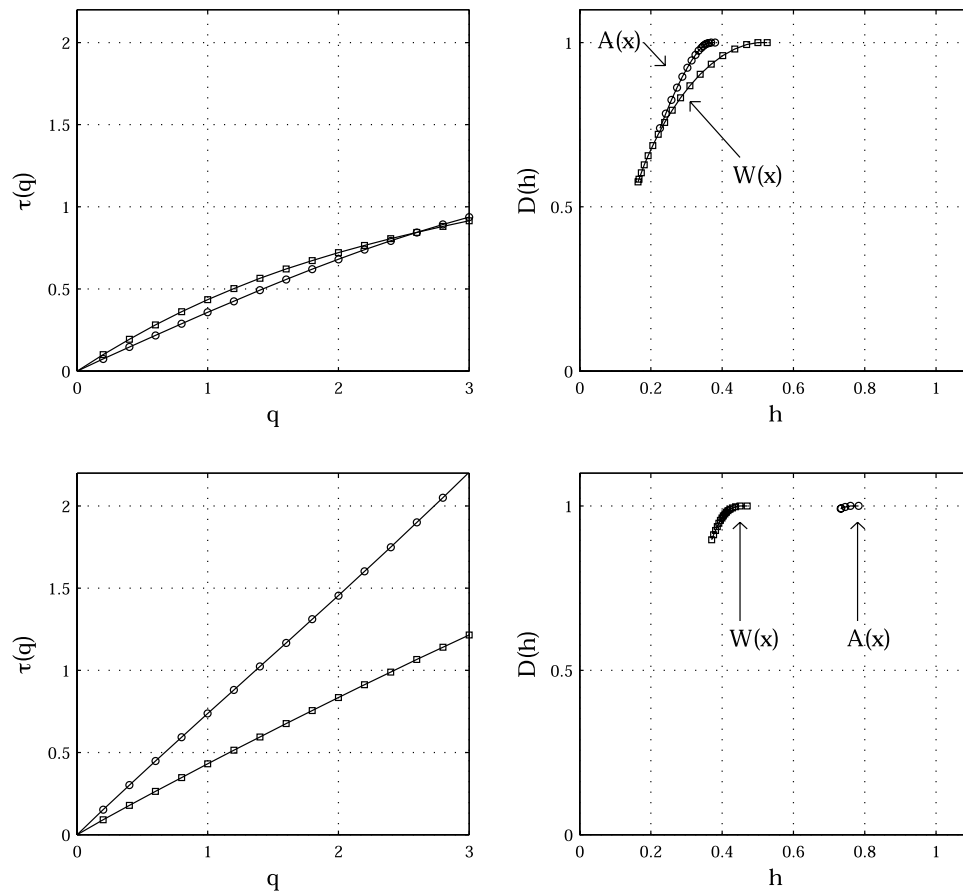


Figure 15. Area function versus width function: (left) scaling exponents $\tau(q)$ and (right) singularity spectra $D(h)$ of area $A(x)$ (circles) and width $W(x)$ (squares) functions computed with CWT coefficients (wavelet g_0^4) for (top) Walawe River basin and (bottom) Noyo River basin.

non-space-filling simulated trees and does it hold for real river networks?

7.2. Area $A(x)$ Versus Width $W(x)$ Function

[79] Our analysis suggests that the area function $A(x)$ of different real networks possesses distinctly different MF properties, whose meaning needs to be carefully interpreted. For the three basins analyzed, the larger Walawe basin was found to have $A(x)$ with $c_1 \simeq 0.4$ and $c_2 \simeq 0.03$ which are distinctly different from those of the much smaller, steeper and still tectonically active California basins ($c_1 \simeq 0.8$ and $c_2 \simeq 0.05$ to 0.10). To rule out the possibility that the unusually large value of $c_1 = 0.8$ is the result of the 1m DEM resolution, the results were confirmed with area functions extracted from DEMs of 1m and 10m DEMs. Our analysis also indicates that the $A(x)$ and $W(x)$ functions of the same basin possess distinctly different MF properties depicting the different drainage topologies of the main river network and the hillslope drainage paths. For example, for the Noyo River basin, we found $c_1 \simeq 0.8$ for $A(x)$ versus $c_1 \simeq 0.5$ for $W(x)$, while for the Walawe basin $c_1 \simeq 0.4$ for $A(x)$ versus $c_1 \simeq 0.5$ for $W(x)$.

[80] However, several questions remain unanswered, such as the following.

[81] 1. What is the effect of DEM resolution and the channel initiation criterion for river network extraction (critical threshold area versus a slope-area threshold) on

the MF properties of $W(x)$? Notice that these questions have been studied before in the literature but with limited MF analysis methodologies as discussed in 4.3 and have to be repeated with the proposed more robust methodology.

[82] 2. When the DEM resolution is small enough (1m to 10 m DEMs) and is able to resolve hillslope flow paths, does in general $A(x)$ emerge as “less rough” than $W(x)$ as was suggested by the two very high resolution basins we analyzed? Note that when the DEM resolution is low, we found that the MF properties of $A(x)$ and $W(x)$ were approximately the same (and in fact $A(x)$ was slightly “rougher” than $W(x)$), but this might be due to the inability of 90 m DEMs to resolve hillslope flow paths and thus to “see” the hillslope drainage patterns.

[83] 3. Can the MF properties of $W(x)$ and $A(x)$ be classified according to basin size as suggested by

Table 5. Comparison Between $A(x)$ and $W(x)$ ^a

		Walawe River	Noyo River
$A(x)$	c_1	0.37	0.77
	c_2	0.06	0.11
$W(x)$	c_1	0.51	0.46
	c_2	0.13	0.10

^aCumulant exponents are computed with CWT coefficients (wavelet g_0^4) for the Walawe River basin and the Noyo River basin.

Richards-Pecou [2002]? While our results do not contradict this hypothesis, we believe that factors other than basin size are at work. Although it is possible that large-scale forcing due to boundary constraints spill over to all other smaller scales of landscape dissection, basin slope, drainage density, geology, etc. might play a role in the MF properties of river networks. A comprehensive analysis using the proposed methodology would provide insight into this problem.

[84] 4. How do two different branching topologies, say one corresponding to the river network at larger scales and another corresponding to the hillslope path topology at smaller scales, mix to give rise to the MF properties of $A(x)$? Can this problem be studied theoretically via constructed multiscale mixed-topology networks?

[85] 5. Do the MF properties of $A(x)$, mostly dominated by the hillslope flow paths, relate to the MF properties of the River Corridor Widths (RCW) introduced by *Gangodagamage et al.* [2007] to directly depict the hillslope topography roughness?

7.3. Hydrologic Implications

[86] Finally, one wonders whether the multiscaling property of area and width functions, apart from a geometrical interpretation related to flow path topology, can be given any hydrological significance. Recently, *Richards-Pecou* [2002] suggested that the multiscaling structure of the area function (actually the author refers to the width function but analyzes the area function) might associate to the scaling structure of at-site flood peaks and can thus serve for regionalization purposes. Specifically, the conjecture was made that the one parameter of the universal multifractals (the Levy-stable α parameter) might relate to the heaviness of the tails of the distributions of floods (see also *Dodov and Foufoula-Georgiou* [2005] for fitted Levy-stable pdfs to maximum annual floods). This is a plausible hypothesis, but one has to be careful with the chosen parameterization of multifractality; in our study we chose a nonparametric class of models as opposed to the universal multifractals used by *Richards-Pecou* [2002] and thus no direct comparison can be made.

[87] Some preliminary ideas on a different hydrologic interpretation of the MF structure of $W(x)$ are offered in this paper. Recalling that $W(x)$ denotes the number of channels intersected by a contour of equal length x to the outlet, $|W(x + \delta x) - W(x)|$ can be interpreted as the net number of channels within a strip of flow distance δx to the outlet. First, the presence of multifractality (c_2 different than zero) implies a strong dependence of the statistics of $|W(x + \delta x) - W(x)|$ on the size of the strip (scale) δx and especially a coefficient of variation of this pdf which increases as the scale δx decreases. That is, there is a disproportionately larger net change in the number of channels (or drainage pathways) expected to appear or disappear in the network at smaller distances apart than at larger distances apart (the larger the value of c_2 the larger this dependence on scale is). On the basis of the above argument, it is clear that the values of c_1 and c_2 are directly related to the scale-dependent probability distribution of the number of in-phase hillslope hydrographs joining the network within a strip of size δx from the outlet, thus expected to affect the properties of the overall hydrograph at the outlet. It is suggested that this scale dependence of $W(x)$ should be further explored toward a scale-dependent convolution

framework for routing and toward alternative explanations of geomorphologic dispersion using higher-order moments of river network topology.

Appendix A: Singularity Spectrum

[88] A MF function $f(x)$ is described as a collection of local singularities, i.e., $|x - x_0|^{h(x_0)}$ whose strength is characterized by the Hölder exponent. The Hölder exponent $h(x_0)$ is properly defined as follows (these definitions actually hold for $h < 1$ but easily extent to $h \geq 1$):

$$h(x_0) = \text{Sup}\{\alpha : f \in C^\alpha(x_0)\}, \quad (\text{A1})$$

where

$$f \in C^\alpha(x_0) \text{ if } |f(x) - f(x_0)| \leq A|x - x_0|^\alpha \quad (\text{A2})$$

for $|x - x_0| \leq \epsilon$. The Hölder exponent can be interpreted as follows: the closer $h(x_0)$ is to 0, the more irregular the function is at point x_0 . In contrast, larger values for $h(x_0)$ are related to a smoother (more regular) behavior at x_0 . For a MF function, the Hölder exponents are spatially distributed on interwoven fractal subsets

$$S(h) = \{x_0 : h(x_0) = h\}, \quad (\text{A3})$$

where $S(h)$ is the collection of points with Hölder exponent h . An efficient framework to characterize MF functions with a hierarchical classification of the subsets $E(h)$ is by using the Hausdorff dimension of these subsets [see, e.g., *Schroeder*, 1991]:

$$D(h) = \text{Dim}_H S(h). \quad (\text{A4})$$

[89] The function $D(h)$ is called the singularity spectrum of the function $f(x)$ and its estimation is the goal of MF analysis.

[90] Monofractal functions are an important subclass of MF functions for which the Hölder exponent takes everywhere the same value H and then the singularity spectrum reduces to a single point: $D(h) = 1$ if $h = H$ and $D(h) = -\infty$ if $h \neq H$ (by convention, $D(\emptyset) = -\infty$ if \emptyset denotes the empty set). A well known example of monofractal process is the ordinary Brownian motion, for which $H = 0.5$. MF functions have a $D(h)$ curve which spans a range of Hölder exponents from h_{\min} to h_{\max} . The MF formalism [*Parisi and Frisch*, 1985] relates $D(h)$ to the spectrum of scaling exponents $\tau(q)$ describing how the statistical moments of fluctuations change with scale.

[91] A similar description can be made for positive measures (or distributions) $\mu(x)$ which are mathematical objects defined through their integral over any interval of \mathbb{R} : $x \rightarrow \int_0^x \mu(u) du$ defines an increasing function which may not possess any derivative. A measure is also described as a collection of singularities: $\int_{x_0-r/2}^{x_0+r/2} \mu(u) du \sim r^{h(x_0)}$ with Hölder exponent $h(x_0)$ defined as

$$h(x_0) = \text{Sup}\{\alpha : \mu \in C^\alpha(x_0)\}, \quad (\text{A5})$$

where

$$\mu \in C^\alpha(x_0) \text{ if } \int_{x_0-r/2}^{x_0+r/2} \mu(u)du \leq Ar^\alpha \quad (\text{A6})$$

for $r \leq \epsilon$. Except for the Hölder exponent definition and the Legendre transform definition (see equation (12)), the MF framework for measures is the same as the one for functions.

[92] **Acknowledgments.** We would like first to acknowledge Julien Beresticky (Laboratoire d'Analyse, de Topologie et de Probabilités, University of Provence, Marseille, France) for fruitful discussions on the link between the Shreve's random network area function process and the Feller diffusion process. Chandana Gangodagamage (St. Anthony Falls Laboratory and National Center for Earth-Surface Dynamics, Department of Civil Engineering, University of Minnesota, Minneapolis, Minnesota, United States) provided us with the area and width functions extracted from DEM data of the Walawe River, Noyo River and South Fork Eel basins. Stéphane Roux (Laboratoire de Physique, École Normale Supérieure de Lyon, Lyon, France) made available to us the codes implementing the WTMM methodology. Finally, we would like to thank Paola Passalacqua for a thorough review of the manuscript and many useful suggestions. This work has been partially supported by the National Center for Earth-Surface Dynamics (NCED), a Science and Technology Center funded by NSF under agreement EAR-0120914. Computer resources were provided by the Minnesota Supercomputing Institute, Digital Technology Center, at the University of Minnesota.

References

- Agnese, C., A. Criminisi, and F. D'Asaro (1998), Scale invariance properties of the peak of the width function in topologically random networks, *Water Resour. Res.*, *34*, 1571–1583.
- Arneodo, A., E. Bacry, and J. Muzy (1995), The thermodynamics of fractals revisited with wavelets, *Physica A*, *213*, 232–275.
- Arneodo, A., S. Manneville, and J. Muzy (1998), Towards log-normal statistics in high Reynolds number turbulence, *Eur. Phys. J. B*, *1*, 129.
- Cui, G., B. Williams, and G. Kuczera (1999), A stochastic Tokunaga model for stream networks, *Water Resour. Res.*, *35*, 3139–3147.
- Delour, J., J. Muzy, and A. Arneodo (2001), Intermittency of 1d velocity spatial profiles in turbulence: A magnitude cumulant analysis, *Eur. Phys. J. B*, *23*, 243–248.
- Dodov, B., and E. Foufoula-Georgiou (2005), Fluvial processes and stream-flow variability: Interplay in the scale-frequency continuum and implications for scaling, *Water Resour. Res.*, *41*, W05005, doi:10.1029/2004WR003408.
- Etheridge, A. (2000), *An Introduction to Superprocesses*, Am. Math. Soc., Providence, R. I.
- Feller, W. (1966), *An Introduction to Probability Theory and Its Applications*, vol. 2, John Wiley, Hoboken, N. J.
- Frisch, U. (1995), *Turbulence: The Legacy of A. N. Kolmogorov*, Cambridge Univ. Press, New York.
- Gangodagamage, C., E. Barnes, and E. Foufoula-Georgiou (2007), Scaling in river corridor widths depicts organization in valley morphology, *Geomorphology*, *43*, doi:10.1016/j.geomorph.2007.04.414.
- Gupta, V. K., and O. Mesa (1988), Runoff generation and hydrologic response via channel network geomorphology—Recent progress and open problems, *J. Hydrol.*, *102*, 3–28.
- Gupta, V., and E. Waymire (1996), Multiplicative cascades and spatial variability in rainfall, river networks, and floods, in *Reduction and Predictability of Natural Disasters*, edited by J. B. Rundle, D. L. Turcotte, and W. Klein, Santa Fe Inst. Stud. Sci. Complexity, vol. 25, Addison-Wesley, Boston, Mass.
- Gupta, V. K., E. Waymire, and I. Rodriguez-Iturbe (1986), On scales, gravity, and network structure in basin runoff, in *Scale Problems in Hydrology*, edited by V. K. Gupta, I. Rodriguez-Iturbe, and E. F. Wood, pp. 159–184, D. Reidel, Hingham, Mass.
- Hasley, T., M. Jensen, L. Kadanoff, I. Procaccia, and B. Shraiman (1986), Fractal measures and their singularities: The characterization of strange sets, *Phys. Rev. A*, *33*, 413–423.
- Horton, R. (1945), Erosional development of streams and their drainage basins: Hydrophysical approach to quantitative geomorphology, *Geol. Soc. Am. Bull.*, *56*, 275–370.
- Jaffard, S. (1997), Multifractal formalism for functions, *SIAM J. Math. Anal.*, *28*(4), 944–998.
- Jaffard, S., B. Lashermes, and P. Abry (2005), Wavelet leaders in multifractal analysis, paper presented at 4th International Conference on Wavelet Analysis and Its Applications, Univ. of Macao, Macao, China.
- Kirkby, M. (1976), Tests of random model and its application to basin hydrology, *Earth Surf. Processes Landforms*, *1*, 197–212.
- Lashermes, B. (2005), Practical multifractal analysis: Wavelet leaders and critical orders. Applications to fully developed turbulence. Finite Reynolds number effects, Ph.D. thesis, Ecole Normale Super. de Lyon, Lyon, France.
- Lashermes, B., P. Abry, and P. Chainais (2004), New insights into the estimation of scaling exponents, *Int. J. Wavelets Multiresolut. Inf. Process.*, *2*(4), 497–523.
- Malécot, Y., C. Auriault, H. Kahalerras, Y. Gagne, O. Chanal, B. Chabaud, and B. Castaing (2000), A statistical estimator of turbulence intermittency in physical and numerical experiments, *Eur. Phys. J. B*, *16*, 549–561.
- Mallat, S. (1998), *A Wavelet Tour of Signal Processing*, Academic, San Diego, Calif.
- Mandelbrot, B., and T. Viscek (1989), Directed recursive models for fractal growth, *J. Phys. A Math. Gen.*, *22*, L377–L383.
- Marani, M., R. Rigon, and A. Arneodo (1991), A note on fractal channel networks, *Water Resour. Res.*, *27*, 3041–3049.
- Marani, M., A. Rinaldo, R. Rigon, and I. Rodríguez-Iturbe (1994), Geomorphological width functions and the random cascade, *Geophys. Res. Lett.*, *21*, 2123–2126.
- Menabde, M., S. Veitzer, V. Gupta, and M. Sivapalan (2001), Test of peak flow scaling in simulated self-similar river networks, *Adv. Water Resour.*, *24*, 991–999.
- Montgomery, D., and W. Dietrich (1988), Where do channels begin?, *Nature*, *336*, 232–234.
- Montgomery, D., and E. Foufoula-Georgiou (1993), Channel networks representation using digital elevation models, *Water Resour. Res.*, *29*, 1925–1934.
- Muzy, J., E. Bacry, and A. Arneodo (1993), Multifractal formalism for fractal signals: The structure-function approach versus the wavelet-transform modulus-maxima method, *Phys. Rev. E*, *47*, 875–884.
- Muzy, J., E. Bacry, and A. Arneodo (1994), The multifractal formalism revisited with wavelets, *Int. J. Bifurcation Chaos*, *4*, 245–302.
- Parisi, G., and U. Frisch (1985), On the singularity structure of fully developed turbulence, in *Turbulence and Predictability in Geophysical Fluid Dynamics, Proc. Int. Summer Sch. Phys. Enrico Fermi*, vol. 88, edited by M. Ghil, R. Benzi, and G. Parisi, pp. 84–88, Elsevier, New York.
- Peano, G. (1890), Sur une courbe qui remplit toute une aire plane, *Mat. Ann.*, *36*, 157–160.
- Peckham, S. (1995), New results for self-similar trees with applications to river networks, *Water Resour. Res.*, *31*, 1023–1029.
- Richards-Pecou, B. (2002), Scale invariance analysis of channel network width function and possible implications for flood behavior, *Hydrol. Sci. J.*, *47*(3), 387–404.
- Rinaldo, A., I. Rodríguez-Iturbe, R. Rigon, E. Ijjasz-Vasquez, and R. Bras (1993), Self-organized fractal river networks, *Phys. Rev. Lett.*, *70*, 822–825.
- Rodriguez-Iturbe, I., and A. Rinaldo (1997), *Fractal River Basins. Chance and Self-Organization*, Cambridge Univ. Press, New York.
- Schroeder, M. (1991), *Fractals, Chaos, Power Laws. Minutes from an Infinite Paradise*, W. H. Freeman, New York.
- Shreve, R. (1966), Statistical laws of stream numbers, *J. Geol.*, *74*, 17–37.
- Sklar, L. S., W. E. Dietrich, E. Foufoula-Georgiou, B. Lashermes, and D. Bellugi (2006), Do gravel bed river size distributions record channel network structure?, *Water Resour. Res.*, *42*, W06D18, doi:10.1029/2006WR005035.
- Strahler, A. (1957), Quantitative analysis of watershed geomorphology, *Eos Trans. AGU*, *38*, 913.
- Tokunaga, E. (1978), Consideration on the composition of drainage networks and their evolution, *Geogr. Rep. 13*, Tokyo Metropol. Univ., Tokyo.
- Troutman, B., and M. Karlinger (1984), On the expected width function for topologically random channel networks, *J. Appl. Probab.*, *21*, 836–849.
- Troutman, B., and M. Karlinger (1985), Unit hydrograph approximations assuming linear flow through topologically random channel networks, *Water Resour. Res.*, *21*, 743–754.
- Troutman, B., and T. Over (2001), River flow mass exponents with fractal channel networks and rainfall, *Adv. Water Resour.*, *24*, 967–989.
- Veneziano, D., E. Glenn, and R. Bras (1995), Multifractal analysis: Pitfalls of standard procedures and alternatives, *Phys. Rev. E*, *52*, 1387–1398.

Venugopal, V., S. Roux, E. Foufoula-Georgiou, and A. Arneodo (2006a), Scaling behavior of high resolution temporal rainfall: New insights from a wavelet-based cumulant analysis, *Phys. Lett. A*, 348, 335–345.

Venugopal, V., S. G. Roux, E. Foufoula-Georgiou, and A. Arneodo (2006b), Revisiting multifractality of high-resolution temporal rainfall using a wavelet-based formalism, *Water Resour. Res.*, 42, W06D14, doi:10.1029/2005WR004489.

Yang, D., S. Herath, and K. Musiak (2001), Spatial resolution sensitivity of catchment geomorphologic properties and the effect on hydrological simulation, *Hydrol. Processes*, 15, 2085–2099.

E. Foufoula-Georgiou and B. Lashermes, St. Anthony Falls Laboratory and National Center for Earth-Surface Dynamics, Dept. of Civil Engineering, University of Minnesota–Twin Cities, 23rd Ave SE, Minneapolis, MN 55414, USA. (efi@umn.edu)